

Narrow-linewidth short-pulse III-V-on-silicon mode-locked lasers based on a linear and ring cavity geometry

S. Keyvaninia,^{1,2} S. Uvin,^{1,2} M. Tassaert,^{1,2,7} X. Fu,^{1,2} S. Latkowski,³ J. Mariën,⁴ L. Thomassen,⁴ F. Lelarge,⁵ G. Duan,⁵ P. Verheyen,⁶ G. Lepage,⁶ J. Van Campenhout,⁶ E. Bente,³ G. Roelkens^{1,2,3,*}

¹Photonics Research Group, Department of Information Technology, Ghent University – imec, B-9000, Belgium

²Center for Nano- and Biophotonics (NB-Photonics), Ghent University, Ghent B-9000, Belgium

³Photonic Integration group, Eindhoven University of Technology, Den Dolech 2, Eindhoven, The Netherlands

⁴Antwerp Space, Berkenrodelei 33, 2260 Hoboken, Belgium

⁵III-V lab, a joint lab of 'Alcatel-Lucent Bell Labs France', 'Thales Research and Technology' and 'CEA Leti', Campus Polytechnique, 1, Avenue A. Fresnel, 91767 Palaiseau cedex, France

⁶imec, Kapeldreef 75, B-3001 Leuven, Belgium

⁷currently at Calipso – Huawei, Ghent B-9000, Belgium

*gunther.roelkens@intec.ugent.be

Abstract: Picosecond-pulse III-V-on-silicon mode-locked lasers based on linear and ring extended cavity geometries are presented. In passive mode-locked operation a 12 kHz –3dB linewidth of the fundamental RF tone at 4.7 GHz is obtained for the linear cavity geometry and 16 kHz for the ring cavity geometry. Stabilization of the repetition rate of these devices using hybrid mode-locking is also demonstrated.

©2015 Optical Society of America

OCIS codes: (060.5625) Radio frequency photonics; (250.5300) Photonic integrated circuits; (140.4050) Mode-locked lasers.

References and links

1. G. C. Valley, "Photonic analog-to-digital converters," *Opt. Express* **15**(5), 1955–1982 (2007).
 2. T. Yilmaz, C. DePriest, T. Turpin, J. Abeles, and P. Delfyett, "Toward a photonic arbitrary waveform generator using a modelocked external cavity semiconductor laser," *IEEE Photon. Technol. Lett.* **14**(11), 1608–1610 (2002).
 3. J. Yao, "Microwave Photonics," *J. Lightwave Technol.* **27**(3), 314–335 (2009).
 4. V. Moskalenko, S. Latkowski, S. Tahvili, T. de Vries, M. Smit, and E. Bente, "Record bandwidth and sub-picosecond pulses from a monolithically integrated mode-locked quantum well ring laser," *Opt. Express* **22**(23), 28865–28874 (2014).
 5. S. Latkowski, V. Moskalenko, S. Tahvili, L. Augustin, M. Smit, K. Williams, and E. Bente, "Monolithically integrated 2.5 GHz extended cavity mode-locked ring laser with intracavity phase modulators," *Opt. Lett.* **40**(1), 77–80 (2015).
 6. S. Srinivasan, M. Davenport, M. Heck, J. Hutchinson, E. Norberg, G. Fish, and J. Bowers, "Low phase noise hybrid silicon mode-locked lasers," *Frontiers in Optoelectronics* 14010-SS.3d (2014).
 7. S. Keyvaninia, M. Muneeb, S. Stanković, P. J. Van Veldhoven, D. Van Thourhout, and G. Roelkens, "Ultra-thin DVS-BCB adhesive bonding of III-V wafers, dies and multiple dies to a patterned silicon-on-insulator substrate," *Opt. Mater. Express* **3**(1), 35–46 (2013).
 8. S. Keyvaninia, G. Roelkens, D. Van Thourhout, C. Jany, M. Lamponi, A. Le Liepvre, F. Lelarge, D. Make, G.-H. Duan, D. Bordel, and J.-M. Fedeli, "Demonstration of a heterogeneously integrated III-V/SOI single wavelength tunable laser," *Opt. Express* **21**(3), 3784–3792 (2013).
 9. D. Vermeulen, Y. De Koninck, Y. Li, E. Lambert, W. Bogaerts, R. Baets, and G. Roelkens, "Reflectionless grating couplers for Silicon-on-Insulator photonic integrated circuits," *Opt. Express* **20**(20), 22278–22283 (2012).
 10. Y. Li, D. Vermeulen, Y. De Koninck, G. Yurtsever, G. Roelkens, and R. Baets, "Compact grating couplers on silicon-on-insulator with reduced backreflection," *Opt. Lett.* **37**(21), 4356–4358 (2012).
 11. F. Laghezza, F. Scotti, P. Ghelfi, and A. Bogoni, "Photonics-Assisted Multiband RF Transceiver for Wireless Communications," *J. Lightwave Technol.* **32**(16), 2896–2904 (2014).
-

1. Introduction

Semiconductor mode-locked lasers generating short (~picosecond) optical pulses at GHz repetition rates are of interest in a range of applications, including photonics-assisted analog-to-digital converters [1], arbitrary waveform generation [2] and microwave photonics [3], due to their compact size, low power consumption and ruggedness. Low-noise performance is of paramount importance in such applications. Fundamentally, the noise performance is determined by the spontaneous emission generated in the amplifier section of the mode-locked laser. Therefore, limiting the length of the semiconductor optical amplifier and realizing a low-loss optical cavity, consisting for a large part out of passive waveguides is crucial. This can be realized on a III-V semiconductor platform by active-passive integration [4,5]. However, the passive waveguide losses on a III-V semiconductor platform are typically in the 2-3 dB/cm range, thereby inducing substantial loss when long cavities (low repetition rates) are required. Replacing the III-V passive waveguide circuit by a silicon photonic integrated circuit can reduce the cavity loss (provided the III-V to silicon coupling structure is low loss), due to the well-developed CMOS fabrication technology used to realize such waveguides. Moreover, at telecom wavelengths also the two-photon absorption losses are substantially lower in silicon compared to InP-based waveguides, thereby creating less excess loss related to the high peak power nature of the optical pulses traveling in the mode-locked laser cavity. Integration of such mode-locked lasers on a silicon photonics platform also allows the integration of low insertion loss filters, high-speed optical modulators and detectors together with the mode-locked laser, allowing the realization of complex high-speed photonic integrated circuits, potentially in large volume. This fact was also recognized by others, demonstrating low phase noise hybrid silicon mode-locked lasers both in ring-based configuration and linear cavity arrangement, both with and without optical feedback to reduce the phase noise / jitter of the generated pulse train [6]. 3dB radiofrequency linewidths of 1.5 MHz (at 20 GHz repetition rate), 52 kHz (at 19.9 GHz repetition rate), 250 kHz (at 18.32 GHz repetition rate) and 15 kHz (at 9.95 GHz repetition rate) were obtained in a ring-based configuration, a ring-cavity configuration with intra-cavity filter, a linear cavity arrangement without feedback (and with cleaved laser facets) and with on-chip feedback respectively [6]. In this paper we describe III-V-on-silicon mode-locked lasers based on low-loss silicon waveguide circuits (0.7dB/cm at 1550nm wavelength), resulting in a narrow linewidth / low phase noise operation. In passive mode-locked operation a 12 kHz -3 dB linewidth of the fundamental RF tone at 4.7 GHz is obtained for the linear cavity geometry and 16 kHz for the ring cavity geometry (36 kHz and 49 kHz -10 dB linewidth respectively). Optical pulses as short as 1.5 ps are obtained. The devices are also studied in the hybrid mode-locking regime. In this case the phase noise spectrum of the fundamental RF tone follows that of the local oscillator used to hybridly mode-lock the device up to several 100 kHz.

2. III-V and silicon waveguide structure and processing

A schematic cross-section of the III-V-on-silicon waveguide structure is shown in Fig. 1. The silicon photonic components are defined in a 400 nm thick silicon waveguide layer using 193 nm deep UV lithography on 200 mm silicon-on-insulator wafers, using a 180 nm deep dry etch. The silicon waveguide circuits are planarized through SiO₂ deposition and chemical mechanical polishing down to the silicon device layer. The III-V layer stack is bonded to this silicon waveguide circuit using DVS-BCB adhesive bonding, using a 40 nm thick bonding layer [7]. The III-V epitaxial layer stack that is used consists of a 200 nm thick n-InP contact layer, two 100 nm thick InGaAsP separate confinement heterostructure layers (bandgap wavelength 1.17 μ m), 6 InGaAsP quantum wells (6 nm thick, emission wavelength 1.55 μ m) surrounded by InGaAsP barriers, a 1.5 μ m thick p-InP top cladding (graded doping from 5×10^{18} to 5×10^{17} cm⁻³) and a 300 nm p + + InGaAs contact layer. The optical coupling between the silicon device layer and the III-V epitaxial stack is realized using a spotsize

converter by tapering both the III-V mesa and silicon waveguide as described in [8]. The semiconductor optical amplifier / saturable absorber mesa width is 3 μm . The total III-V taper length is 150 μm , tapering from 3 μm down to 0.5 μm width. The silicon waveguide tapers up from 300 nm waveguide width. The III-V saturable absorber is realized in the same active material as the gain section and is isolated from the gain section by a dry etch 200 nm into the p-InP cladding layer. The confinement factor of the optical mode in the multi-quantum well stack is 7.5% both in the gain section and in the saturable absorber. The propagation loss of the silicon waveguide (650 nm wide) was measured through a cut-back experiment and is 0.7 dB/cm in the 1550nm wavelength range.

A key technological step to realize high-performance III-V-on-silicon lasers based on this scheme is the definition of the 500 nm III-V taper tip. While 500 nm critical dimensions are trivial for silicon photonic integrated circuits, this is far less the case for the high-aspect-ratio III-V waveguides, defined using contact lithography. In this work, such narrow taper tips are defined using 320 nm UV contact lithography and controlled wet chemical etching of the III-V epitaxial layer stack, demonstrating the manufacturability of these components in standard III-V processing lines. A SiN mask was defined using 320 nm UV contact lithography. The mask is 1 μm wide at the taper tip. In a first step the InGaAs layer is etched using reactive ion etching (RIE). Afterwards the InP p-doped layer and the MQW stack are etched using selective wet chemical etching with 1HCl:1H₂O and 1H₂SO₄:1H₂O₂:3H₂O respectively. A photoresist mask was used to protect the InGaAs contact layer during MQW wet etching. By carefully selecting the orientation of the amplifier mesa with respect to the III-V crystal orientation (mesas along the [01-1] crystal direction), a negative sidewall slope of $\sim 10^\circ$ can be achieved in the anisotropic etching of InP, reaching a 500nm width at the multi-quantum well active region. After III-V mesa etching the n-InP layer is etched away using HCl, except where n-type contacts are required. GeAu/Ni was used for the n-contacts. The III-V structure is then encapsulated with DVS-BCB and the TiAu p-contact is deposited after opening the DVS-BCB on top of the III-V mesa.

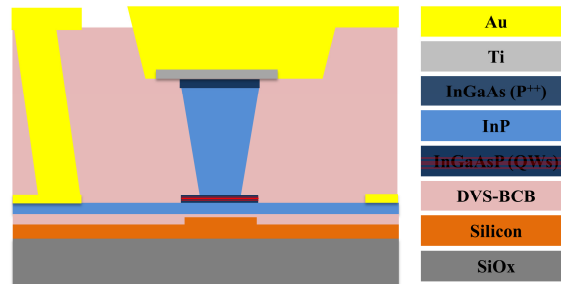


Fig. 1. Cross-section of the III-V-on-silicon waveguide structure.

3. Linear cavity III-V-on-silicon mode-locked lasers

The linear III-V-on-silicon mode-locked laser cavity is schematically depicted in Fig. 2(a) and 2(b). It consists of a III-V waveguide section consisting of two spotsizer converters as described above, 2 semiconductor optical amplifier sections and 1 saturable absorber section, placed symmetrically in the laser cavity in order to obtain colliding pulse operation. The cavity mirrors are formed by first order distributed Bragg reflectors (255nm grating period, 50% duty cycle, 180nm etch depth). 7 periods were used for both mirrors, leading to a reflectivity of about 50% over the wavelength range of interest. The semiconductor optical amplifier sections are 2x430 μm long (not including the 150 μm long spotsizer converters) while the saturable absorber is 100 μm long. The remainder of the laser cavity consists of a $\sim 2 \times 0.7$ cm long low-loss silicon waveguide (symmetrically placed around the III-V section) in order to reach ~ 5 GHz repetition rate in colliding pulse mode. A microscope image of the

fabricated device is shown in Fig. 2(c). The spotsizer converters and both SOAs share the same p-contact for ease of electrical contacting. The p-side electrical isolation between the SOA and the saturable absorber is 50 k Ω . All III-V sections, including the saturable absorber, share the same n-contact.

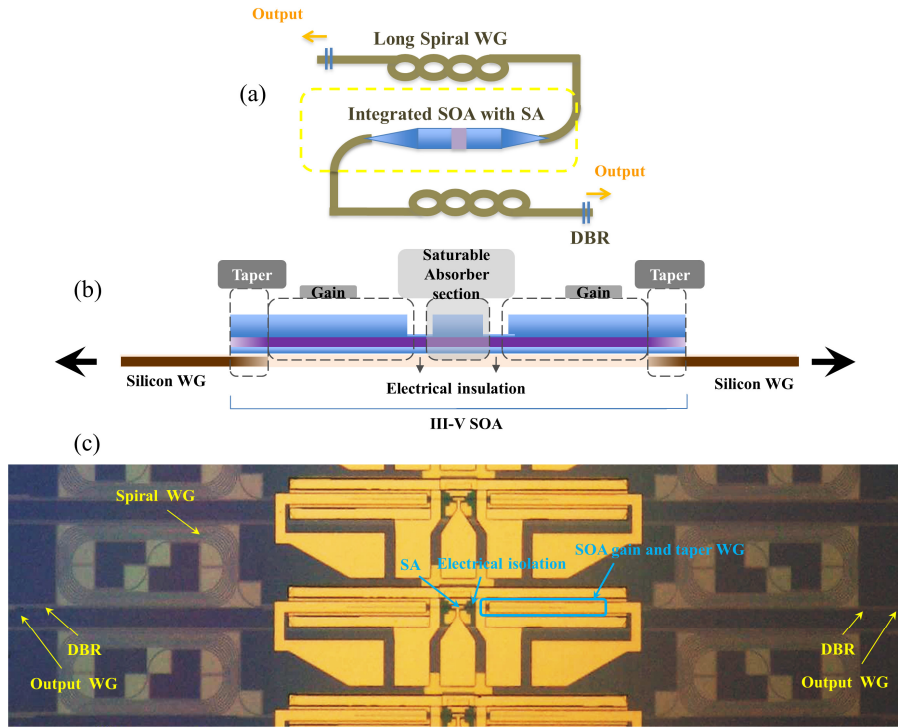


Fig. 2. Schematic top-view (a) and longitudinal cross-section (b) of the linear cavity colliding pulse mode-locked laser geometry. A microscope image of the fabricated device is shown in (c).

The output of the mode-locked laser was coupled to an optical fiber through a fiber-to-chip grating coupler, 3 mm away from the laser outcoupling mirror. The light-versus-current curve (fiber coupled optical power) of this device is shown in Fig. 3, as a function of saturable absorber reverse bias. The fiber-to-chip coupling efficiency is measured to be -12 dB. The back-reflection of the grating coupler is below -20 dB. The erratic behavior in the light-versus-current curve is attributed to parasitic back-reflections from the grating coupler into the laser cavity. In order to reduce the parasitic back-reflections a dedicated grating coupler structure can be used with -50 dB back-reflection as analyzed and demonstrated in [9] and [10] respectively.

For the passive mode-locking experiments, the saturable absorber is reverse biased at -1.2 V and 160 mA current is injected in the spotsizer converters and semiconductor optical amplifiers. The optical fiber was either connected to a high-resolution optical spectrum analyzer (20 MHz resolution), a high-speed photodiode (50 GHz bandwidth) that was connected to a 50 GHz electrical spectrum analyzer or a second harmonic generation based intensity autocorrelator (SHG-AC), after passing through an EDFA. An optical isolator was used to prevent back-reflections into the laser. The measurements were carried out with the device on a thermo-electric cooler set at 20 $^{\circ}$ C. The measurements results are presented in Fig. 4. Figure 4(a) shows the high-resolution optical spectrum generated by the mode-locked laser. A 9 nm -3 dB optical bandwidth is obtained.

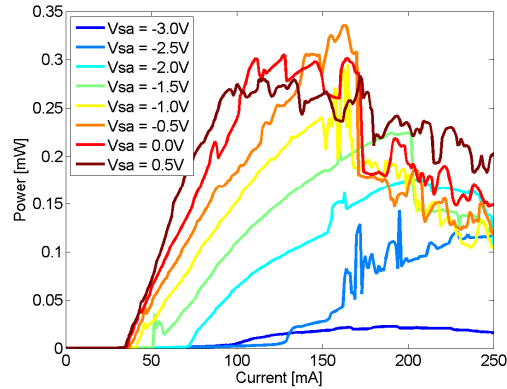


Fig. 3. Light-current curve for the linear cavity arrangement as a function of the saturable absorber reverse bias (fiber coupled output power).

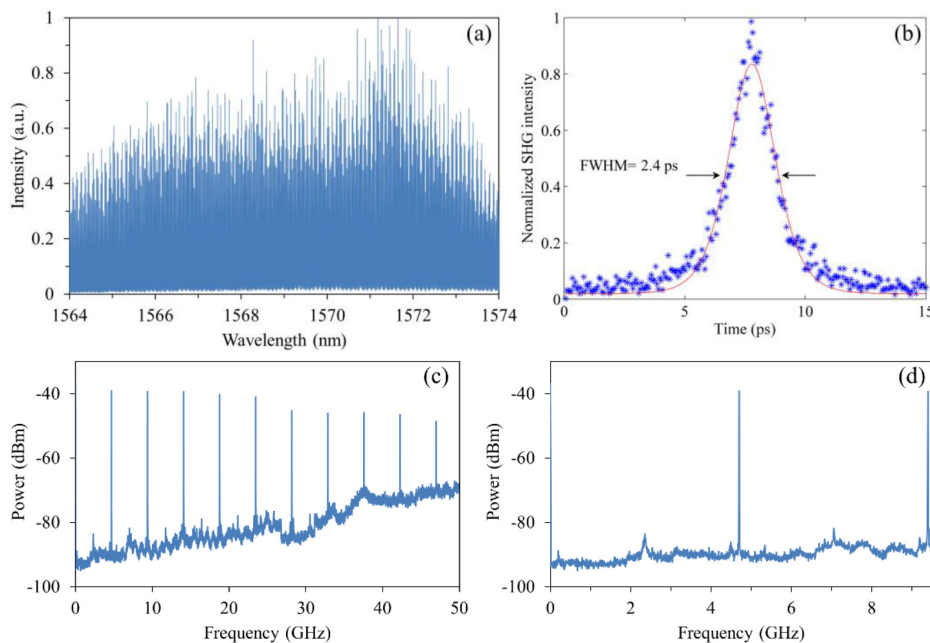


Fig. 4. (a) High resolution optical spectrum using a resolution bandwidth of 20 MHz; (b) intensity autocorrelation trace of the pulse train; (c) wide span electrical spectrum of the generated pulse train; (d) zoom of the electrical spectrum from baseband to the second harmonic illustrating strong suppression of the tone at half the repetition rate of the colliding pulse mode-locked laser. Resolution bandwidth, video bandwidth and sweep time used to obtain the RF spectra were 500 kHz, 50 kHz, and 1.5 s for (c), and 100 kHz, 10 kHz, and 7.5 s for (d) respectively. The laser gain section was biased at 160 mA, while the saturable absorber had a reverse bias of -1.2 V.

Using the SHG-AC the pulse duration was determined to be 1.5 ps assuming a sech^2 pulse shape as shown in Fig. 4(b), using a correction factor of 1.54 between the full width at half maximum (FWHM) of the SHG-AC trace and the actual pulse width. A wide frequency span electrical spectrum is shown in Fig. 4(c) and a detailed spectrum from baseband to the second harmonic is shown in Fig. 4(d). As can be seen in Fig. 4(d) a residual component at half the repetition rate can be observed, however more than 40 dB below the main RF tone, illustrating good colliding pulse operation of the device. The linewidth and phase noise spectrum of the 4.69 GHz fundamental RF tone was also assessed. For these measurements

the power supplies for the amplifiers and saturable absorbers were filtered using large capacitors (~ 100 mF) ensuring the elimination of noise contributions by this equipment. Figure 5(a) shows a detailed electrical spectrum indicating a 36 kHz -10 dB bandwidth (12 kHz -3 dB linewidth), an improvement to previously reported values from similar III-V-on-silicon mode-locked lasers. Figure 5(b) shows the phase noise spectrum of the main RF tone from 10 Hz to 10 GHz from the carrier frequency. The total integrated jitter from 50 kHz to 10 MHz is 2.56 ps.

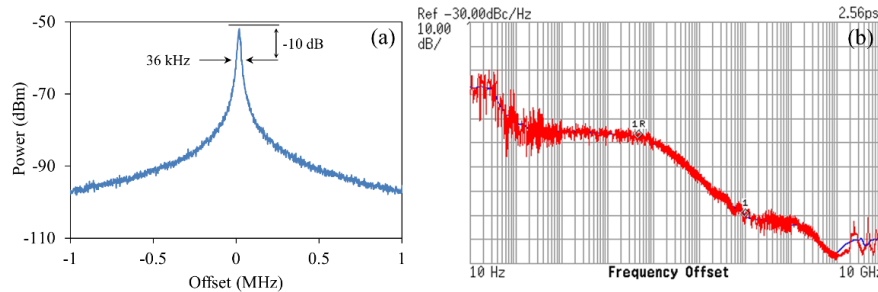


Fig. 5. (a) Zoom of the main RF tone, indicating a 36 kHz -10 dB bandwidth; (b) phase noise spectrum of the main RF tone at 4.69 GHz. The timing jitter is 2.56 ps when integrated from 50 kHz to 10 MHz. Resolution bandwidth, video bandwidth and sweep time used to obtain the RF spectra in (a) were 2 kHz, 20 Hz, and 40 s respectively.

Hybrid mode-locking of the linear cavity mode-locked laser was also investigated. The saturable absorber was reverse biased at -1.1 V and a local oscillator signal at 4.7 GHz (12 dBm RF power at the source) was delivered to the saturable absorber using a bias-T. Hybrid mode-locking was obtained and the wide band electrical spectrum together with the phase noise of the 4.7 GHz component is shown in Fig. 6. The total integrated jitter from 50 kHz to 10 MHz is improved to 353 fs. The phase noise spectrum of the fundamental component follows that of the local oscillator in the measurement range of 10 Hz to 200 kHz.

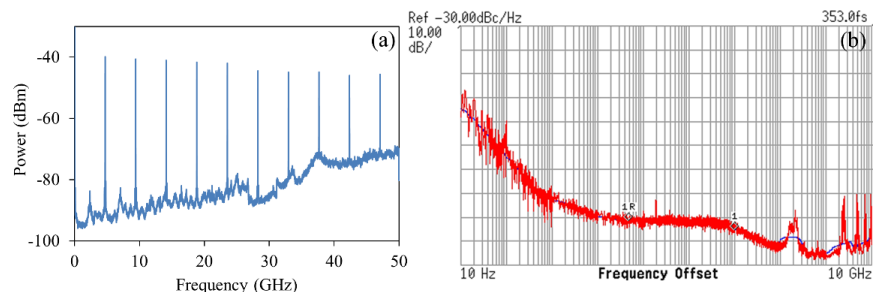


Fig. 6. (a) Wide band electrical spectrum under hybrid mode-locking; (b) phase noise spectrum of the main RF tone at 4.7 GHz under hybrid mode-locking. The timing jitter is 353 fs when integrated from 50 kHz to 10 MHz. Resolution bandwidth, video bandwidth and sweep time used to obtain the RF spectra in (a) were 500 kHz, 50 kHz, and 1.5 s respectively.

4. Ring cavity III-V-on-silicon mode-locked laser

While linear cavity arrangements allow stable colliding pulse mode-locking, a residual tone at half the repetition rate of the laser can be found. Depending on the operating point this can be more or less suppressed. In high-end applications such as microwave photonics, the occurrence of such spurious signals is undesirable. The residual tone originates from the fact that two pulses travel in the laser cavity and couple to the same output. If these two pulses are not identical, a spurious tone occurs. Such spurious tones can therefore be avoided by using ring cavities: in this case also two pulses travel inside the laser cavity (clockwise and counterclockwise), but they couple to a different output waveguide. The layout of the studied

ring cavity mode-locked lasers is shown in Fig. 7 together with a microscope image of the fabricated device. The semiconductor optical amplifier sections are $2 \times 790 \mu\text{m}$ long (not including the $150 \mu\text{m}$ long spotsizer converters) while the saturable absorber is $180 \mu\text{m}$ long. The remainder of the laser cavity consists of a $\sim 1.3 \text{ cm}$ long low-loss silicon waveguide in order to reach 5 GHz repetition rate. The optical coupling between the ring cavity and a silicon bus waveguide is done through a directional coupler (35% power coupling). The spotsizer converters and both SOAs share the same p-contact for ease of electrical contacting. The p-side electrical isolation between the SOA and the saturable absorber is $50 \text{ k}\Omega$. All III-V sections, including the saturable absorber, share the same n-contact. For the passive mode-locking experiments, the saturable absorber is reverse biased at -1.3 V and 179 mA current is injected in the spotsizer converters and semiconductor optical amplifiers.

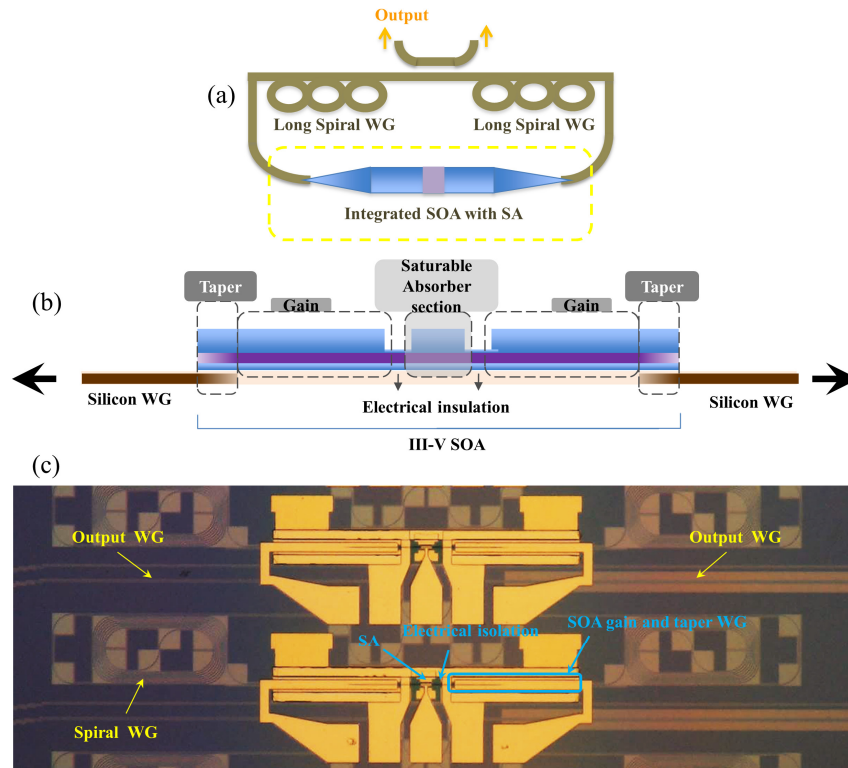


Fig. 7. Schematic top-view (a) and longitudinal cross-section (b) of the ring cavity mode-locked laser geometry. A microscope image of the fabricated device is shown in (c).

Identical measurements were carried out as in the case of the linear cavity device. The output of the mode-locked laser was coupled to an optical fiber through a fiber-to-chip grating coupler, 4 mm away from the laser outcoupling mirror. The light-versus-current curve (fiber coupled optical power) of this device is shown in Fig. 8 as a function of saturable absorber reverse bias. The fiber-to-chip coupling efficiency is measured to be -12 dB . The back-reflection of the grating coupler is below -20 dB . The erratic behavior in the light-versus-current curve is again attributed to parasitic back-reflections from the grating coupler into the laser cavity. Figure 9(a) shows the high-resolution optical spectrum generated by the mode-locked laser. A 2.5 nm 3 dB optical bandwidth and 7 nm 10 dB optical bandwidth is obtained. Figure 9(b) shows the intensity autocorrelator trace. The pulse shape is not bell-shaped as in the linear cavity arrangement. This is attributed to the existence of additional features around the main pulse such as leading or trailing satellite peaks, attributed to partial incoherence of the laser comb spectrum, the source of which is not fully understood. A wide frequency span

electrical spectrum is shown in Fig. 9(c) and a detailed spectrum from baseband to the second harmonic tone is shown in Fig. 9(d). No spurious tone is observed at half the laser repetition rate, as can be expected from these ring cavity structures. The linewidth and phase noise spectrum of the main RF tone was also assessed (again using large decoupling capacitors to stabilize the power supplies). Figure 10(a) shows a zoom of the main RF tone, indicating a 49 kHz -10 dB bandwidth (16kHz -3 dB bandwidth). Figure 10(b) shows the phase noise spectrum of the main RF tone. The total integrated jitter from 50 kHz to 10 MHz is 1.65 ps.

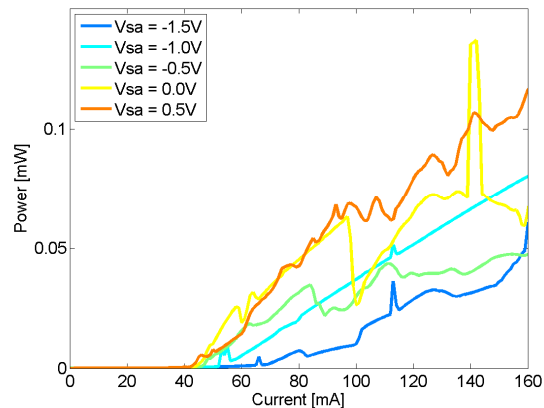


Fig. 8. Light-current curve for the ring cavity arrangement as a function of the saturable absorber reverse bias (fiber coupled output power).

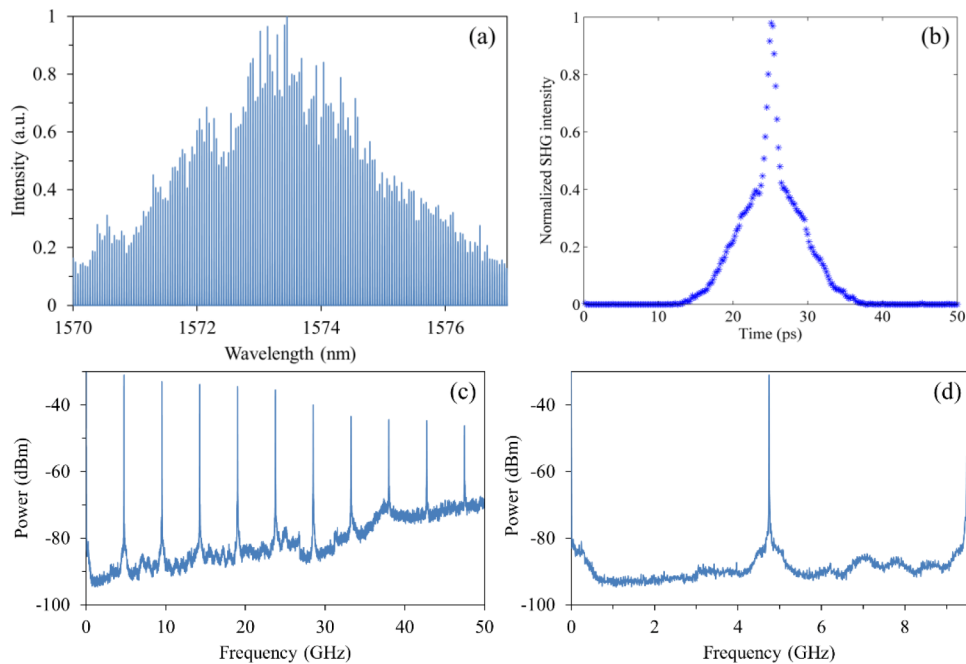


Fig. 9. (a) High resolution (20 MHz) optical spectrum; (b) autocorrelation trace of the optical output; (c) wide span electrical spectrum of the generated pulse train; (d) zoom of the electrical spectrum from baseband to the second harmonic illustrating a clean spectrum between the RF harmonics in the case of a ring-cavity mode-locked laser geometry. Resolution bandwidth, video bandwidth and sweep time used to obtain the RF spectra were 500 kHz, 50 kHz, and 1.5s for (c), and 100 kHz, 10 kHz, and 7.5 s for (d) respectively. The laser gain section was biased at 179 mA, while the saturable absorber had a reverse bias of -1.3 V.

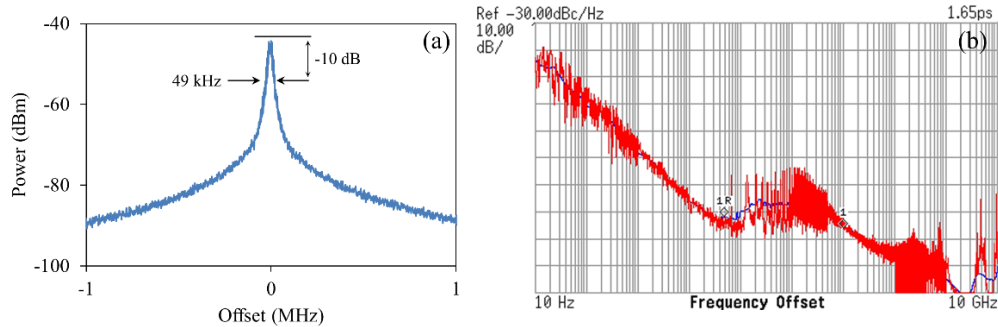


Fig. 10. (a) Zoom of the main RF tone, indicating a 49 kHz -10 dB bandwidth; (b) phase noise spectrum of the main RF tone at 4.72 GHz. Resolution bandwidth, video bandwidth and sweep time used to obtain the RF spectra in (a) were 2 kHz, 20 Hz, and 40 s respectively.

Hybrid mode-locking of the ring-cavity mode-locked laser was also investigated. The saturable absorber was reverse biased at -1.4 V and a local oscillator signal at 4.65 GHz (15 dBm RF power from the source) was delivered to the saturable absorber using a bias-T. Hybrid mode-locking was obtained and the wide band electrical spectrum and the phase noise of the 4.65 GHz component is shown in Fig. 11. The total integrated jitter from 50 kHz to 100 MHz is reduced to 817 fs. The phase noise spectrum of the fundamental component follows that of the local oscillator in the measurement range of 10 Hz to 300 kHz.

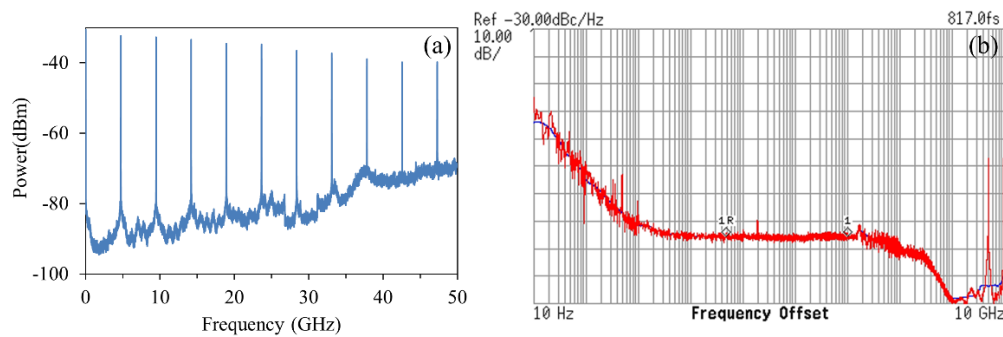


Fig. 11. (a) Wide band electrical spectrum under hybrid mode-locking; (b) phase noise spectrum of the main RF tone at 4.65 GHz under hybrid mode-locking. Resolution bandwidth, video bandwidth and sweep time used to obtain the RF spectra in (a) were 500 kHz, 50 kHz, and 1.5 s respectively.

5. Conclusion

In this paper narrow linewidth, short-pulse III-V-on-silicon mode-locked lasers using a grating coupler based fiber-to-chip interface are presented. These devices can be used in more complex photonic integrated circuits, such as photonics-assisted analog to digital converters, arbitrary waveform generation and microwave photonics functions such as frequency down-converters and up-converters [11]. The implementation of these devices on a silicon photonic platform with 400 nm silicon waveguide layer thickness enables the co-integration of these devices with high-speed silicon modulators and photodetectors. Using such a platform also high performance lower repetition rate (longer cavity) mode-locked lasers can be implemented.

Acknowledgments

This work was carried out in the framework of the European Space Agency “Electro-Photonic Frequency Converter” project.